Control of Structure and Dynamics in Polymer-Networked Engineered Nanoparticle Arrays by Electric Fields

Xingfei Wei and Ewa Harazinska
Department of Chemistry, Johns Hopkins University, Baltimore, Maryland 21218, USA

Rigoberto Hernandez*
Department of Chemistry, Johns Hopkins University, Baltimore, Maryland 21218, USA
Department of Chemical & Biomolecular Engineering,
Johns Hopkins University, Baltimore, Maryland 21218, USA and
Department of Materials Science and Engineering,
Johns Hopkins University, Baltimore, Maryland 21218, USA
(Dated: October 14, 2023)

Polymer-networked nanoparticles are the basis for advanced materials useful wearable electronics, drug delivery, autonomous computing and other applications. To characterize and predict the physics and underlying mechanisms of the network connections in 2D and 3D engineered nanoparticle (ENP) arrays, we developed an analogous Potts model of 3-state sites. Together with dissipative particle dynamics (DPD) simulations, we found that the network structures in polymer-linked nanoparticle assemblies are generally dominated by the number of nearest neighbors and not the topology of the lattice. When the E-field regulates the network connections, the links along the E-field direction always dominate the overall network structure.

Polymer-based complex networked materials have applications in a variety of areas, [1–5] such as stretchable bioelectronics, [6] self-healing materials, [7] gas separation, [8] drug delivery, [9–11] high performance materials with strong mechanical properties, [12–15] and autonomous computing materials. [16, 17] For example, a high performance electronic material consisting of a stretchable polymer network and electrical conductive polymers has been seen to achieve the strong mechanical properties and high electrical conductivity needed to realize an electronic skin. [6] The controlled release of a peptide drug has been realized by applying a hydrogel network made of oxidized starch nanoparticles (NPs) and carboxymethyl chitosan. [18] Different types of logic gates have also been realized using percolated networks made of silver micro-flakes and thermoplastic polyurethane. [17] The properties of these advanced materials are directly related to their corresponding network structures.

Computational methods play an important role in uncovering the fundamental structure-property relationships in complex materials through theoretical models, [19–23] Molecular Dynamics (MD), [24–30] Monte Carlo (MC), [24, 31] and Machine Learning (ML) methods. [32] Combining experiments and mathematical modeling, Yu *et al.* [21] found that the temperature dependent mechanical properties in polymer-NP networks are associated with combined entropy-driven and enthalpy-driven mechanisms. The bond lifetime in dynamic polymer networks has been determined through rheology and dielectric spectroscopy experiments together with the lifetime renormalized analytical model. [19, 20] The effects of polymer chain length and connection bonding energy on rheology properties of polymer networks were revealed through MD and MC.[24] MD simulations together with network models have revealed thermal transport mechanisms in amorphous polymers and polymer composites. [27, 28] Moreover, unique phononic applications of thermal networks have been seen when heat flux is regulated spatio-temporally. [22, 23] Our recent simulations have also indicated that 2D regular square arrays of polymer linked engineered nanoparticle (ENP) networks have potential applications in brain-like data storage and computing. [16, 29, 30] As noted in Ref. [29], regular arrays of nanoparticles in 2D can be fabricated by e-beam lithography, nanosphere lithography, and self-assembly of polymer grafted nanoparticles.[33, 34] In three dimensions, DNA-coated nanoparticles have been shown to assemble into regular lattices in which the nanoparticles are sufficiently far apart that additional polymer links could be formed and regulated by external drivers such as temperature and external fields. [35] In parallel, 2D regular square arrays have been fabricated in experiments and exhibited plasmonic switching regulated by temperature or pH changes. [36]

Revealing the physics of dynamic network connections is critical to predicting network structures in complex systems. [1] Using thermodynamic perturbation theory and a colloidal particle simulations, Howard *et al.* [25, 26] reported that the phase behavior and structural properties of polymer-NP networks were affected by polymer molecular weight, concentration, and flexibility. Combining transmission electron microscopy (TEM), small-angle X-ray scattering (SAXS) experiments and reverse MC simulations, Musino *et al.* [31] characterized the network structures in silica NP and styrene-butadiene composites. However, their simple hard sphere model did not account for the elastic properties of the polymer tethered

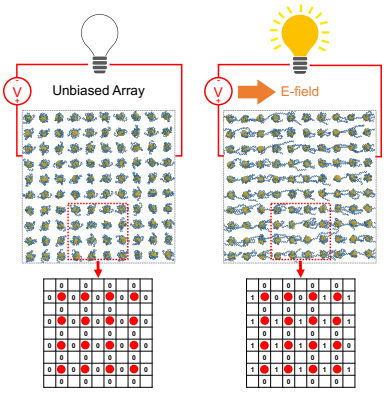

FIG. 1. Scheme of electric field induced network structure changing in 2D SQ regular arrays. The detailed simulation model is described in Ref. [29] and Fig. S1 in [37].

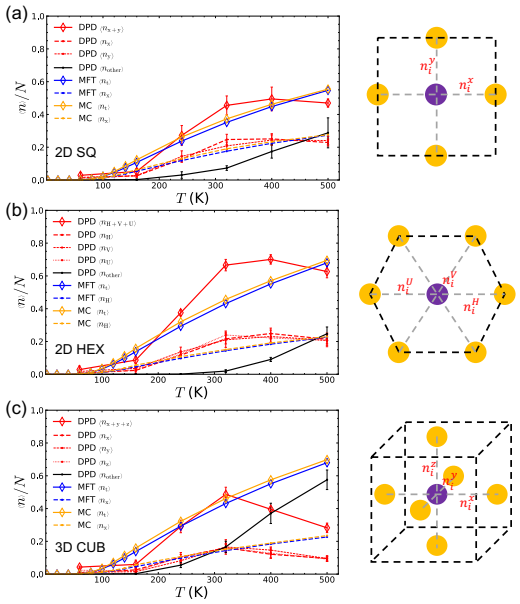

FIG. 2. Comparisons of network connections in (a) 2D SQ, (b) 2D HEX, (c) and 3D CUB at T ranging from 30 to 500 K under no E-field. Observations of DPD simulations are compared to the Potts model from MFT and MC. Diamond symbols represent the sum of nearest neighbor links. Small dots represent nearest neighbor links in each direction. Black solid lines represent other types of links. The normalization factor N is the total number of ENPs in the array; here, N = 100 in both 2D SQ and 2D HEX, N = 125 in 3D CUB.

silica NPs which might lead to different quantitative and qualitative behavior. One alternative would be to use ML methods to propagate such large complex networks with high accuracy [32], but it comes at the price of hiding the physics within the machine.

In this work, we developed a Spin-Ising Potts model with 3-state spins to describe the complex network connections in polymer linked soft materials. The Potts model is generalizable from 2D to 3D architectures. We also use Dissipative Particle Dynamics (DPD) models to simulate polymer network connections in different regular arrays of ENPs—*viz.* 2D Square (SQ), 2D Hexagonal (HEX), 3D Simple Cubic (CUB), and 3D Hexagonal Close Packing (HCP) structure; see Scheme S1 in [37]. We use the DPD force field to simulate poly(allylamine hydrochloride)s (PAHs). [38–43] Both Coulombic and Lennard-Jones potentials are used to model gold nanoparticle (AuNP) and PAH interactions.[39–41, 44, 45] Implicit solvent environment is applied by setting the dielectric constant to 80 and using the Langevin thermostat. The simulation model was optimized according to experimental [13, 46–48] and simulation [39, 49, 50] benchmarks. The Large-scale Atomic Molecular Massively Parallel Simulator (LAMMPS) package [51] is used to conduct all MD simulations; see Fig. S1 in [37] for simulation details. The Potts models implemented here describe simplified networks limited to nearest neighbor links in 2D SQ, 2D HEX, and 3D CUB arrays shown in Schemes S1 and S2 in [37], and is amenable to Mean Field Theory (MFT) and MC. [29, 52] More importantly, we have demonstrated that the network connection can be regulated by an external E-field using both Potts model and DPD simulations; see Fig. 1. This ENP network property is an experimentally accessible order parameter which has been used for characterization and control in drug delivery, [9–11] wearable electronics, [6] and computing materials.[16]

The positions of link n in the selected arrays are noted in Schemes. S1 and S2 in [37]. A link site takes on values $\{0, 1, -1\}$ when there is no link, a directed link from left to right and a link from right to left, respectively; see Scheme. S3 in [37]. The full Hamiltonians, $\mathcal{H}^{\mathrm{SQ}}\left(n^x_{i,j}, n^y_{i,j}\right)$, $\mathcal{H}^{\mathrm{HEX}}\left(n^{\mathrm{H}}_{i,j}, n^{\mathrm{V}}_{i,j}, n^{\mathrm{U}}_{i,j}\right)$ and $\mathcal{H}^{\mathrm{CUB}}\left(n^x_{i,j,k}, n^y_{i,j,k}, n^z_{i,j,k}\right)$ are provided in the methods section in SM [37], and are characterized by three effective energies, ϵ_1, ϵ_2 and ϵ_{E}, corresponding to the activation of links, the interaction between neighbor links, and the applied field, respectively. Their values are kept constant across different arrays to allow for direct comparison. The resulting MFT Hamiltonians are available in SM [37]; for the 2D square array, it takes the form,

$$\begin{aligned} h^{\mathrm{SQ}}_{\mathrm{MFT}}(n_x, n_y) = \epsilon_1(|n_x| + |n_y|) + \\ \epsilon_2 |n_x| * 2(m_x + 2m_y) + \\ \epsilon_2 |n_y| * 2(m_y + 2m_x) + \\ \epsilon_{E_x} * n_x \end{aligned} \tag{1}$$

where m_x is the mean-field estimate of the average links in the x-direction which results from taking the mean of the effective force on the link sites.

The MFT equations for the Potts model are solved by considering a representative linking site for each of the the linking directions; *e.g.* in 2D SQ, there are two link sites, n_x and n_y. MC for Potts model is performed by

applying the full Hamiltonian on the same regular arrays as in DPD model; *e.g.* 10×10 2D SQ array. The correspondence between the DPD and Potts models is established by fixing the parameters $\{\epsilon_\alpha\}$ in Eq. 1 such that the MFT predictions match DPD at intermediate temperatures; see Fig. 2 and Fig. S2 in [37]. The resulting values are $\epsilon_1 = 1.0\,\text{kcal/mol}$, $\epsilon_2 = 0.4$ kcal/mol, and ϵ_E varies from -0.6 to -1.2 kcal/mol. Notably, the activation energy is at the same order of magnitude with that in Ref. 24 which found bonding energy equal to a few $k_\text{B}T$ in an analogous polymer network. Without E-field, the network structure is isotropic but depends on temperature. The E-field creates a symmetry breaking that can align (or drive the formation of) links; see Fig. 1 and Scheme S2 in [37].

We compare DPD to MFT and MC in Fig. 2 for cases with no applied E-field. The mean connectivity is connected to the overall transfer of energy or electrons across the network. In isotropic network systems, the mean connectivity represents the overall network structure, because there is no preferred direction. More details for the 2D SQ model are available in Fig. S3 in [37]. Although our Potts model only considers nearest neighbors, we find that MFT and MC generally capture the DPD behavior in 2D SQ; see Fig. 2 (a). At high temperatures, $T > 400$ K, DPD simulations exhibit a large number of links beyond the nearest neighbors, which cannot be captured by the Potts model by its construction. We also observe that MFT and MC agree better at low temperatures, but MFT over-predicts at high temperatures as expected from its overestimation of neighbor interactions.

We also report results for the 2D HEX and 3D CUB models from DPD and Potts models in Figs. 2 (b) and (c), respectively. Additional observables are available in Figs. S4-S5 in [37]. Without E-field, we find agreement in the 2D HEX array for the mean link occupancy across each of the directions, $\langle n_\text{H}\rangle$, $\langle n_\text{V}\rangle$ and $\langle n_\text{U}\rangle$ at different temperatures, confirming that the network structure is isotropic. This symmetry was also confirmed for the 3D CUB array in Fig. 2 (c) from the agreement between $\langle n_\text{x}\rangle$, $\langle n_\text{y}\rangle$ and $\langle n_\text{z}\rangle$.

Although the network connection energy could vary across the 2D SQ, 2D HEX and 3D CUB arrays, here the energy constants in the corresponding Potts models are set the same. We found that in the Potts model, MFT and MC for both 2D HEX and 3D CUB still agree with DPD. For example, in 2D HEX, the nearest links, $\langle n_\text{H}\rangle$, $\langle n_\text{V}\rangle$ and $\langle n_\text{U}\rangle$ match with MFT and MC very well. In 3D CUB, the nearest links, $\langle n_\text{x}\rangle$, $\langle n_\text{y}\rangle$ and $\langle n_\text{z}\rangle$, match well with MFT and MC, up to $T \sim 320$ K, but we also see deviations $T \sim 400 - 500$ K. in Fig. 2 (c). This arises because the Potts model only includes nearest neighbor links, and the DPD model makes a significant number of other links at high temperatures, $T > 320$ K.

Increases in the non-nearest neighbor links was seen to reduce the nearest neighbor links in the DPD simulations.

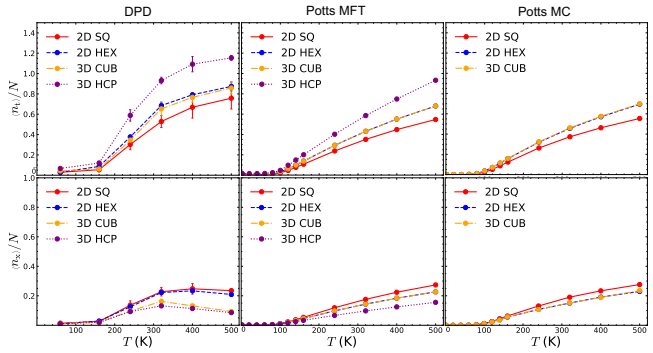

FIG. 3. Comparison of links across 2D SQ, 2D HEX, 3D CUB, and 3D HCP arrays. The 1st, 2nd and 3rd columns correspond to DPD, Potts model MFT, and Potts model MC, respectively. The first row reports the total numbers of links. The second row reports the average number of links in the x-direction. The normalization factor $N = 100$, 100, 125, and 180 in 2D SQ, 2D HEX, 3D CUB, and 3D HCP, respectively. The other links and sum of nearest neighbor links from DPD simulations are available in Fig. S7 in [37].

As the PAH chains have more space to move in 3D CUB than in 2D HEX, the number of other links in 3D CUB is also larger than in 2D HEX at 500 K.

Figure 3 compares the number of links for the 2D SQ, 2D HEX, 3D CUB and 3D HCP zero-field models at different temperatures. In this limit, the temperature driven network structures are isotropic. We use averaged x-link numbers for the comparison in different arrays. The 2D SQ, 2D HEX and 3D CUB arrays in Fig. 2 have 4, 6 and 6 nearest neighbors next to each ENP and each link is a nearest neighbor to 6, 10 and 10 other links, respectively. The network structures in 2D HEX are quite different from those in 3D CUB. The 3D HCP array has not been mapped into Potts model because the latter requires each link to have 22 nearest neighbor links, which leads to a numerically expensive representation. Nevertheless, the behavior of 3D HCP DPD simulations were observed and available in Fig. S6 in [37].

In the DPD and Potts models of the different arrays, we thus find that link numbers increase with increasing temperature as they are activated with increasing frequency; see Fig. 3. The total links in the DPD simulations increase with the number of nearest neighbor links—*viz.* 3D HCP > 3D CUB ∼ 2D HEX > 2D SQ, upper row in Fig. 3. The average links in each direction, shown in the bottom row of Fig. 3, are reduced when the number of nearest neighbor links increases due to the competing interactions between neighbors. Although 2D HEX and 3D CUB have similar $\langle n_\text{total}\rangle$, 2D HEX has larger $\langle n_x\rangle$, while 3D CUB has larger $\langle n_\text{other}\rangle$; see Fig. 3 and Fig. S7 in [37]. Similar to 3D CUB, we also see a significant number of $\langle n_\text{other}\rangle$ in the 3D HCP array in Fig. S7 (a) because the 3D topology gives more free space for the polymer to make other links. Mean-

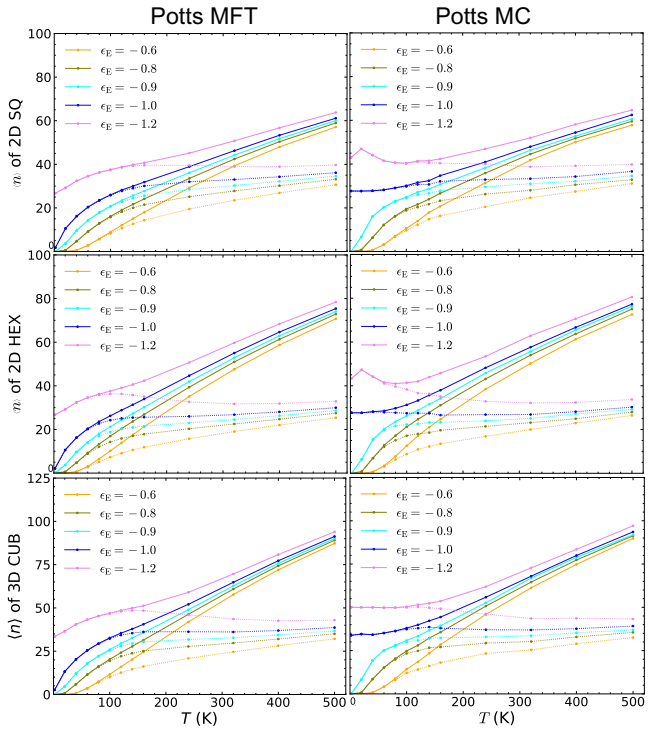

FIG. 4. Total links (solid lines), and links along the E-field x-direction (dotted lines) of the MFT and MC of the Potts model for the 2D SQ and 2D HEX, and 3D CUB arrays driven by a nonzero E-field, $\epsilon_{\rm E}$ varying from -0.6 to -1.2 kcal/mol, at temperatures from $T = 2 - 500$ K. Here $\epsilon_1 = 1.0$ kcal/mol and $\epsilon_2 = 0.4$ kcal/mol are kept constant.

while, more non-neighbor links ($\langle n_{\rm other}\rangle$) are found in 2D SQ than in 2D HEX. The Potts model helps confirm the relationships of the number of total links—*viz.* 3D HCP $>$ 3D CUB $\sim$ 2D HEX $>$ 2D SQ, and the number of nearest neighbor links—*viz.* 3D HCP $<$ 3D CUB $\sim$ 2D HEX $<$ 2D SQ. MFT and MC also predict that both 2D HEX and 3D CUB have fewer links, $\langle n_x\rangle$, than 2D SQ. However, as the Potts model does not account for other links, it cannot capture the corresponding features in DPD. For example, $\langle n_{\rm other}\rangle$ in 3D CUB is much larger than 2D HEX, resulting in a reduction of $\langle n_x\rangle$.

With an E-field applied on the ENP network, all links align along the E-field direction. Although in DPD simulations, upon setting an E-field of $E_x \sim +0.0002$ V/Å, a simulation time of 60 million steps was not long enough to reach equilibrium, we found the links are polarized along the x-axis; see Figs. S8 - S11 in [37]. This property plays a key role in characterizing the degree to which this material is useful for changing and maintaining states, which can be important in enabling autonomous computing.[16] We use MFT and MC solutions from the Potts model to provide theoretical predictions for the E-field polarized network connection link numbers. We choose $\epsilon_{\rm E} = -0.6$ to -1.2 kcal/mol as an approximate E-field strength range using T from 2 K to 500 K for mapping the DPD model; see Fig. 4.

In 2D SQ arrays, the number of total and x-links increase with increasing E-field strength from -0.6 to -1.2 kcal/mol (first row in Fig. 4). At high temperatures, x-links that could be induced by the E-field are suppressed by the isotropic thermal effects. Thus, both MFT and MC predict diminishing network connections in this limit. At low temperatures, the number of x-links is the major contribution to the total links. We found that at 2 K with the magnitude of $\epsilon_{\rm E}$ larger than activation energy $\epsilon_1 = 1.0$ kcal/mol, E-field can activate and induce a polarized network. The MFT approximation did not give rise to a polarized network at 2 K when $\epsilon_{\rm E} = -1.0$ kcal/mol for the neighbor interaction $\epsilon_2 = 0.4$ kcal/mol. However, MC does result in more links as can be seen in comparing the left and right figures in the first row of Fig. 4.

The second and third rows of Figure 4 report the Potts model predictions for 2D HEX and 3D CUB arrays. In general, the observations reported above for 2D SQ are also seen in 2D HEX and 3D CUB arrays. At 2 K $\epsilon_{\rm E} < -1.0$ kcal/mol, the network can be polarized along the x-direction, and the MC method can predict links using the full Hamiltonians—*viz.* $\mathcal{H}^{\rm SQ}\left(n^x_{i,j}, n^y_{i,j}\right)$, $\mathcal{H}^{\rm HEX}\left(n^{\rm H}_{i,j}, n^{\rm V}_{i,j}, n^{\rm U}_{i,j}\right)$ and $\mathcal{H}^{\rm CUB}\left(n^x_{i,j,k}, n^y_{i,j,k}, n^z_{i,j,k}\right)$. MFT also leads to better convergence with increasing number of neighbors and increasing dimensionality in 2D HEX and 3D CUB. However, the MFT approximations deviate more strongly from MC in 2D HEX and 3D CUB, due to the mean-field treatment of nearest neighbor links giving rise to too many neighbor-neighbor interactions and reducing the number of links.

In this paper, we developed a Potts model —*viz.* a Spin Ising model with 3 possible spin states— that captures the network connections in a unique class of soft materials consisting of an array of nanoparticles imbedded in a polymer matrix. The Potts model is generalizable to different 2D and 3D architectures with a simple Hamiltonian of 3 energetic interaction terms. One important finding from this work is that the network connections can be regulated by an external electric field. We found that generic properties of polymer-nanoparticle networks are dominated by the number of nearest neighbors and not the topology of the lattice. Moreover, while increasing the number of nearest neighbors can increase the number of total links, the competing interaction among nearest neighbors leads to a decreasing average number of links to a given neighbor. We also found that when the E-field directs the network connections, the links along the E-field direction always dominate the overall network structure independent of the array topology.

This work has been partially supported by the National Science Foundation (NSF) through Grant No. CHE 2102455. The computing resources necessary for this work were performed in part on Expanse at the San Diego

Supercomputing Center through allocation CTS090079 provided by Advanced Cyberinfrastructure Coordination Ecosystem: Services & Support (ACCESS), which is supported by National Science Foundation (NSF) grants #2138259, #2138286, #2138307, #2137603, and #2138296. Additional computing resources were provided by the Advanced Research Computing at Hopkins (ARCH) high-performance computing (HPC) facilities supported by the NSF MRI Grant (OAC-1920103).

* Correspondence to: r.hernandez@jhu.edu

[1] M. J. Webber and M. W. Tibbitt, Dynamic and reconfigurable materials from reversible network interactions, Nat. Rev. Mater. **7**, 541 (2022).

[2] N. Zheng, Y. Xu, Q. Zhao, and T. Xie, Dynamic covalent polymer networks: A molecular platform for designing functions beyond chemical recycling and self-healing, Chem. Rev. **121**, 1716 (2021).

[3] M. A. Campea, M. J. Majcher, A. Lofts, and T. Hoare, A review of design and fabrication methods for nanoparticle network hydrogels for biomedical, environmental, and industrial applications, Adv. Funct. Mater. **31**, 2102355 (2021).

[4] C. Dannert, B. T. Stokke, and R. S. Dias, Nanoparticle-hydrogel composites: From molecular interactions to macroscopic behavior, Polymers **11**, 275 (2019).

[5] C. Progyateg and D. Konkolewicz, Dynamic covalent bonds in polymeric materials, Angew. Chem., Int. Ed. **131**, 9784 (2019).

[6] Y. Jiang, Z. Zhang, Y.-X. Wang, D. Li, C.-T. Coen, E. Hwaun, G. Chen, H.-C. Wu, D. Zhong, S. Niu, W. Wang, A. Saberi, J.-C. Lai, Y. Wu, Y. Wang, A. A. Trotsyuk, K. Y. Loh, C.-C. Shih, W. Xu, K. Liang, K. Zhang, Y. Bai, G. Gurusankar, W. Hu, W. Jia, Z. Cheng, R. H. Dauskardt, G. C. Gurtner, J. B.-H. Tok, K. Deisseroth, I. Soltesz, and Z. Bao, Topological supramolecular network enabled high-conductivity, stretchable organic bioelectronics, Science **375**, 1411 (2022).

[7] C.-H. Li, C. Wang, C. Keplinger, J.-L. Zuo, L. Jin, Y. Sun, P. Zheng, Y. Cao, F. Lissel, C. Linder, X.-Z. You, and Z. Bao, A highly stretchable autonomous self-healing elastomer, Nat. Chem. **8**, 618 (2016).

[8] C. R. Bilchak, M. Jhalaria, Y. Huang, Z. Abbas, J. Midya, F. M. Benedetti, D. Parisi, W. Egger, M. Dickmann, M. Minelli, F. Doghieri, A. Nikoubashman, C. J. Durning, D. Vlassopoulos, J. Jestin, Z. P. Smith, B. C. Benicewicz, M. Rubinstein, L. Leibler, and S. K. Kumar, Tuning selectivities in gas separation membranes based on polymer-grafted nanoparticles, ACS Nano **14**, 17174 (2020).

[9] R. T. Chacko, J. Ventura, J. Zhuang, and S. Thayumanavan, Polymer nanogels: A versatile nanoscopic drug delivery platform, Adv. Drug Deliv. Rev. **64**, 836 (2012).

[10] Z. Huang, X. Chen, S. J. K. O'Neill, G. Wu, D. J. Whitaker, J. Li, J. A. McCune, and O. A. Scherman, Highly compressible glass-like supramolecular polymer networks, Nat. Mater. **21**, 103 (2021).

[11] A. Chrisnandy, D. Blondel, S. Rezakhani, N. Broguiere, and M. P. Lutolf, Synthetic dynamic hydrogels promote degradation-independent in vitro organogenesis, Nat. Mater. **21**, 479 (2022).

[12] T. L. Sun, T. Kurokawa, S. Kuroda, A. B. Ihsan, T. Akasaki, K. Sato, M. A. Haque, T. Nakajima, and J. P. Gong, Physical hydrogels composed of polyampholytes demonstrate high toughness and viscoelasticity, Nat. Mater. **12**, 932 (2013).

[13] G. P. Baeza, C. Dessi, S. Costanzo, D. Zhao, S. Gong, A. Alegria, R. H. Colby, M. Rubinstein, D. Vlassopoulos, and S. K. Kumar, Network dynamics in nanofilled polymers, Nat. Commun. **7**, 11368 (2016).

[14] R. Nadiv, R. M. F. Fernandes, G. Ochbaum, J. Dai, M. Buzaglo, M. Varenik, R. Biton, I. Furó, and O. Regev, Polymer nanocomposites: Insights on rheology, percolation and molecular mobility, Polymer **153**, 52 (2018).

[15] S. Ge, S. Samanta, B. Li, G. P. Carden, P.-F. Cao, and A. P. Sokolov, Unravelling the mechanism of viscoelasticity in polymers with phase-separated dynamic bonds, ACS Nano **16**, 4746 (2022).

[16] M. Bathe, R. Hernandez, T. Komiyama, R. Machiraju, and S. Neogi, Autonomous computing materials, ACS Nano **15**, 3586–3592 (2021).

[17] C. El Helou, P. R. Buskohl, C. E. Tabor, and R. L. Harne, Digital logic gates in soft, conductive mechanical metamaterials, Nat. Commun. **12**, 1633 (2021).

[18] M. J. Majcher, A. Babar, A. Lofts, A. Leung, X. Li, F. Abu-Hijleh, N. M. B. Smeets, R. K. Mishra, and T. Hoare, In situ-gelling starch nanoparticle (snp)/o-carboxymethyl chitosan (cmch) nanoparticle network hydrogels for the intranasal delivery of an antipsychotic peptide, J. Control. Release **330**, 738 (2021).

[19] E. B. Stukalin, L.-H. Cai, N. A. Kumar, L. Leibler, and M. Rubinstein, Self-healing of unentangled polymer networks with reversible bonds, Macromolecules **46**, 7525 (2013).

[20] S. Ge, M. Tress, K. Xing, P.-F. Cao, T. Saito, and A. P. Sokolov, Viscoelasticity in associating oligomers and polymers: Experimental test of the bond lifetime renormalization model, Soft Matter **16**, 390 (2020).

[21] A. C. Yu, H. Lian, X. Kong, H. L. Hernandez, Jian, and E. A. Appel, Physical networks from entropy-driven non-covalent interactions, Nat. Commun. **12**, 1 (2021).

[22] K. Xiong, Z. Liu, C. Zeng, and B. Li, Thermal-siphon phenomenon and thermal/electric conduction in complex networks, Natl. Sci. Rev. **7**, 270 (2020).

[23] S. Wang, C. Zeng, F. Yang, K. Xiong, and B. Li, Energy diffusion of simple networks under the spatiotemporal thermostats, Eur. Phys. J. B **94**, 1 (2021).

[24] D. Amin, A. E. Likhtman, and Z. Wang, Dynamics in supramolecular polymer networks formed by associating telechelic chains, Macromolecules **49**, 7510 (2016).

[25] M. P. Howard, R. B. Jadrich, B. A. Lindquist, F. Khabaz, R. T. Bonnecaze, D. J. Milliron, and T. M. Truskett, Structure and phase behavior of polymer-linked colloidal gels, J. Chem. Phys. **151**, 124901 (2019).

[26] M. P. Howard, Z. M. Sherman, A. N. Sreenivasan, S. A. Valenzuela, E. V. Anslyn, D. J. Milliron, and T. M. Truskett, Effects of linker flexibility on phase behavior and structure of linked colloidal gels, J. Chem. Phys. **154**, 074901 (2021).

[27] J. Zhou, Q. Xi, J. He, X. Xu, T. Nakayama, Y. Wang, and J. Liu, Thermal resistance network model for heat conduction of amorphous polymers, Phys. Rev. Materials

4, 015601 (2020).
[28] J. Zhong, Q. Xi, J. He, J. Liu, and J. Zhou, Thermal percolation and electrical insulation in composite materials with partially metallic coated fillers, Appl. Phys. Lett. **119**, 211602 (2021).
[29] X. Wei, Y. Zhao, Y. Zhuang, and R. Hernandez, Engineered nanoparticle network models for autonomous computing, J. Chem. Phys. **155**, 214702 (2021).
[30] X. Wei, Y. Zhao, Y. Zhuang, and R. Hernandez, Building blocks for autonomous computing materials: Dimers, trimers and tetramers,, J. Chem. Phys. **154**, 154704 (2021).
[31] D. Musino, A.-C. Genix, E. Chauveau, T. Bizien, and J. Oberdisse, Structural identification of percolation of nanoparticles, Nanoscale **12**, 3907 (2020).
[32] K. Srinivasan, N. Coble, J. Hamlin, T. Antonsen, E. Ott, and M. Girvan, Parallel machine learning for forecasting the dynamics of complex networks, Phys. Rev. Lett. **128**, 164101 (2022).
[33] D. Ji, T. Li, and H. Fuchs, Nanosphere lithography for sub-10-nm nanogap electrodes, Adv. Electron. Mater. **3**, 1600348 (2017).
[34] H. Yun, Y. J. Lee, M. Xu, D. C. Lee, G. E. Stein, and B. J. Kim, Softness-and size-dependent packing symmetries of polymer-grafted nanoparticles, ACS Nano **14**, 9644 (2020).
[35] J. S. Kahn and O. Gang, Designer nanomaterials through programmable assembly, Angew. Chem., Int. Ed. **134**, e202105678 (2022).
[36] B. Liu, X. Lu, Z. Qiao, L. Song, Q. Cheng, J. Zhang, A. Zhang, Y. Huang, and T. Chen, ph and temperature dual-responsive plasmonic switches of gold nanoparticle monolayer film for multiple anticounterfeiting, Langmuir **34**, 13047 (2018).
[37] See Supplemental Material at `urltobeaddedhere` for Detailed Descriptions of Methods and Additional Results.
[38] X. Wei, A. Popov, and R. Hernandez, Electric potential of citrate capped gold nanoparticles is affected by poly(allylamine hydrochloride) and salt concentration, ACS Appl. Mater. Interfaces **14**, 12538–12550 (2022).
[39] G. Chong, E. D. Laudadio, M. Wu, C. J. Murphy, R. J. Hamers, and R. Hernandez, Density, structure, and stability of citrate^{3-} and H_2citrate^{-} on bare and coated gold nanoparticles, J. Phys. Chem. C **122**, 28393 (2018).
[40] G. Chong and R. Hernandez, Adsorption dynamics and structure of polycations on citrate-coated gold nanoparticles, J. Phys. Chem. C **122**, 19962–19969 (2018).
[41] G. Chong, I. U. Foreman-Ortiz, M. Wu, A. Bautista, C. J. Murphy, J. A. Pedersen, and R. Hernandez, Defects in self-assembled monolayers on nanoparticles prompt phospholipid extraction and bilayer curvature-dependent deformations, J. Phys. Chem. C **123**, 27951 (2019).
[42] R. D. Groot, Applications of dissipative particle dynamics, in *Novel methods in soft matter simulations*, Lecture notes in Physics, Vol. 640 (Springer, Berlin, Heidelberg, 2004) pp. 5–38.
[43] P. Español and P. Warren, Statistical mechanics of dissipative particle dynamics, Europhys. Lett. **30**, 191 (1995).
[44] Y. Ahn, J. K. Saha, G. C. Schatz, and J. Jang, Molecular dynamics study of the formation of a self-assembled monolayer on gold, J. Phys. Chem. C **115**, 10668 (2011).
[45] P. K. Ghorai and S. C. Glotzer, Molecular dynamics simulation study of self-assembled monolayers of alkanethiol surfactants on spherical gold nanoparticles, J. Phys. Chem. C **111**, 15857 (2007).
[46] J.-W. Park and J. S. Shumaker-Parry, Structural study of citrate layers on gold nanoparticles: Role of intermolecular interactions in stabilizing nanoparticles, J. Am. Chem. Soc. **136**, 1907 (2014).
[47] A. Rostek, D. Mahl, and M. Epple, Chemical composition of surface-functionalized gold nanoparticles, J. Nanopart. Res. **13**, 4809 (2011).
[48] G. A. Dominguez, S. E. Lohse, M. D. Torelli, C. J. Murphy, R. J. Hamers, G. Orr, and R. D. Klaper, Effects of charge and surface ligand properties of nanoparticles on oxidative stress and gene expression within the gut of *Daphnia magna*, Aquat. Toxicol. **162**, 1 (2015).
[49] G. Brancolini, A. Corazza, M. Vuano, F. Fogolari, M. C. Mimmi, V. Bellotti, M. Stoppini, S. Corni, and G. Esposito, Probing the influence of citrate-capped gold nanoparticles on an amyloidogenic protein, ACS Nano **9**, 2600 (2015).
[50] X. Wei, C. Chen, Y. Zhao, E. Harazinska, M. Bathe, and R. Hernandez, Molecular structure of single-stranded DNA on the ZnS surface of quantum dots, ACS Nano **16**, 6666–6675 (2022).
[51] S. J. Plimpton, Fast parallel algorithms for short-range molecular dynamics, J. Comput. Phys. **117**, 1 (1995), https://www.lammps.org.
[52] L. E. Reichl, *A Modern Course in Statistical Physics*, 4th ed. (Wiley-VCH Verlag GmbH and Co. KGaA, Weinheim, Germany, 2016).